Testing the role of SNe Ia for Galactic chemical evolution of p-nuclei with 2D models and with s-process seeds at different metallicities

C. Travaglio

INAF - Astrophysical Observatory Turin, Strada Osservatorio 20, 10025 Pino Torinese (Turin), Italy

B2FH Association - Turin, Italy

travaglio@oato.inaf.it, claudia.travaglio@b2fh.org

R. Gallino

Dipartimento di Fisica, Università di Torino, Via P.Giuria 1, 10125 Turin, Italy

B2FH Association - Turin, Italy

T. Rauscher

Centre for Astrophysics Research, School of Physics, Astronomy and Mathematics, University of Hertfordshire, Hatfield AL10 9AB, United Kingdom

Department of Physics, University of Basel, 4056 Basel, Switzerland

UK Network for Bridging Disciplines of Galactic Chemical Evolution (BRIDGCE), http://www.astro.keele.ac.uk/bridgce, United Kingdom

F. K. Röpke

Universität Würzburg, Am Hubland, D-97074 Würzburg, Germany

and

W. Hillebrandt

Max-Planck-Institut für Astrophysik, Karl-Schwarzschild-Str. 1, D-85748 Garching bei München, Germany

Received _____; accepted _____

ABSTRACT

The bulk of p isotopes is created in the 'gamma processes' mainly by sequences of photodisintegrations and beta decays in explosive conditions in Type Ia supernovae (SNIa) or in core collapse supernovae (ccSN). The contribution of different stellar sources to the observed distribution of p-nuclei in the Solar System is still under debate. We explore single degenerate Type Ia supernovae in the framework of two-dimensional SNIa delayed-detonation explosion models. Travaglio et al. (2011) (hereafter TRV11) discussed the sensitivity of p-nuclei production to different SNIa models, i.e. delayed detonations of different strength, deflagrations, and the dependence on selected s-process seed distributions. Here we present a detailed study of p-process nucleosynthesis occuring in SNIa with s-process seeds at different metallicities. Based on the delayed-detonation model DDT-a of TRV11, we analyze the dependence of p-nucleosynthesis on the s-seed distribution obtained from different strengths of the ^{13}C-pocket. We also demonstrate that ^{208}Pb-seed alone changes the p-nuclei production considerably. The heavy-s seeds ($140 \leq A < 208$) contribute with about 30-40% to the total light-p nuclei production up to ^{132}Ba (with the exception of ^{94}Mo and ^{130}Ba, to which the heavy-s seeds contribute with about 15% only). Using a Galactic chemical evolution code (see Travaglio et al. 2004) we study the contribution of SNIa to the solar stable p-nuclei. We find that explosions of Chandrasekhar-mass single degenerate systems produce a large amount of p-nuclei in our Galaxy, both in the range of light ($A \leq 120$) and heavy p-nuclei, at almost flat average production factors (within a factor of about 3). We discussed in details p-isotopes such as ^{94}Mo with a behavior diverging from the average, which we attribute to uncertainties in the nuclear data or in SNIa modelling.

Li et al. (2011) find that about 70% of all SNeIa are normal events. If these are

explained in the framework of explosions of Chandrasekhar-mass white dwarfs resulting from the single-degenerate progenitor channel, we find that they are responsible for at least 50% of the p-nuclei abundances in the Solar System.

Subject headings: hydrodynamic, supernovae, nucleosynthesis, p-process

1. Introduction

The origin of heavy nuclei was discussed by Cameron (1957), who called 35 species *excluded isotopes*. Indeed they are outside of both the s and r neutron capture paths, and they are typically 10−1000 times less abundant than the corresponding s- and/or r-isotopes in the Solar System. The origin of p-nuclei was investigated starting with the pioneering work of Cameron (1957) and Burbidge et al. (1957), and later by Audouze & Truran (1975) and Arnould (1976). The first work analyzing the possibility of having efficient photodisintegrations in Chandrasekhar-mass SNIa explosions was published by Howard, Meyer & Woosley (1991). The initial s-seed distribution they used was derived from helium flashes as calculated by Howard et al. (1986). In Figure 2 of that work, the authors claim that they can reproduce the abundance pattern of all p-nuclei, including light-p nuclei, within a factor of about three. However, they obtained an overproduction of ^{74}Se, ^{78}Kr, and ^{84}Sr. The p-process abundances of these three isotopes are very sensitive to the proton density, which the authors considered rather uncertain. They also obtained a rather low production of ^{94}Mo and ^{96}Ru with respect to the other light p-nuclei. A detailed discussion on these light p-nuclei will be given in Section 4 of the present paper. Later Goriely et al. 2002, Goriely et al. 2005, and Arnould & Goriely 2006, analyzed the p-process production in He-detonation models for sub-Chandrasekhar mass WDs. These authors considered as seeds s-process solar abundances. They found Ca to Fe to be overabundant with respect to p-nuclei (with the exception of ^{78}Kr) by a factor of $\simeq$100. They concluded that a He detonation is not an efficient scenario for the production of the bulk Solar-System p-isotopes. Kusakabe et al. (2011) presented p-process nucleosynthesis calculations in a CO-deflagration model of SNIa, i.e., the W7 model of Nomoto et al. (1984). Similar to Howard et al. (1986), they assumed enhanced s-seed distributions using the classical s-process analysis, testing two different mean neutron exposures τ_o, a flat distribution for $\tau_o = 0.30$ mb^{-1}, and a decreasing s-process distribution corresponding to $\tau_o = 0.15$ mb^{-1}.

They noticed that for a flat s-seed enhanced distribution the production factors of light p-nuclei show a strong deficiency in the range ^{78}Se to ^{98}Ru. From this, they concluded that SNIa may have contributed to the enrichment of p-nuclei more effectively than ccSNe.

In our previous TRV11 paper, we obtained a consistent production of p-nuclei in the single-degenerate Chandrasekhar mass WD explosion scenario. We presented two-dimensional hydrodynamic models of SNIa. The corresponding nucleosynthesis was calculated in a post-processing step following the thermal history of Lagrangian tracer particles. We found a significant production of p-nuclei from these stellar explosions, at the same level compared to ^{56}Fe for light as well as heavy p-nuclei. We demonstrated that our model is able to produce light and heavy p-nuclei in one single process. In our analysis, we assumed enhanced s-seed distributions directly obtained from a sequence of thermal pulses in the material accreted onto the exploding white dwarf from a normal companion star (see Gallino et al. 1998). In the context of light-p nuclei production, the major problem discussed in TRV11 is the resulting abundance of ^{94}Mo, found to be far too low relative to the abundances of the other light-p nuclei. We also found an important contribution from p-process nucleosynthesis to ^{80}Kr and ^{86}Sr (originally considered s-only nuclei), to the neutron magic ^{90}Zr, and to the neutron-rich ^{96}Zr (due to neutron captures from the residual abundance of ^{22}Ne during the explosive phase). Concerning the heavy p-isotopes, the s-process nature of ^{152}Gd has been later confirmed by different works on s-process nucleosynthesis (Gallino et al. 1998; Bisterzo et al. 2010), where a predominant s-process origin was demonstrated (see also discussion in TRV11).

In the present paper we investigate for the first time in the literature the effect of metallicity on p-process nucleosynthesis in SNIa, starting with a range of s-seed distributions obtained for different metallicities. Using a simple chemical evolution code (Travaglio et al. 2004), we estimate the contribution of SNIa to the solar p-process composition. The

same study was recently done for radiogenic p-isotopes by Travaglio et al. (2014).

It is currently impossible to discuss the interplay between the role of SNeIa and ccSNe in the production of p-nuclei in the Galaxy. Infact a complete study of p-nucleosynthesis with metallicity is missed for ccSNe. But also from the observational point of view, unfortunatey there is no way to measure observed chemical evolution of p-nuclei since they are too rare with respect to the s- and r-fractions. For example, there are recent attempts to observe elements like Mo and Ru (very debated for p-process nucleosynthesis studies) in field stars of the Galaxy at different metallicities (see e.g. Hansen et al. 2014; Peterson 2013). Only a small fraction of the elements Mo and Ru are p: 14.84% of the total Mo is ^{92}Mo and only 9.25% is ^{94}Mo; for Ru, only 5.5% of the element is ^{96}Ru and 1.88% is ^{98}Ru. The p-fractions indicated above are therefore too small to be of any interest when the elements are observed in field stars. Only when will be possible to observe isotopes of Mo and Ru in the spectra then we will be able to give interesting indications on the details of their nucleosynthesis processes.

For this work, the adopted SNIa model (described in detail in TRV11) is summarized in Section 2, together with a brief description of the tracer particles method used for nucleosynthesis calculations. In Section 3 the s-process seed distributions considered in our study are described in detail. The resulting p-process production and the effect of metallicity on p-nuclei is discussed in Section 4, where also an analysis of the various production mechanisms of the p-nuclei will be performed, taking into account nuclear uncertainties. In Section 5 we analyzed in detail how s-seeds with different atomic mass number contribute to the p-nuclei production. Galactic chemical evolution calculations are presented in Section 6, and the contribution of SNIa to the solar system p-nuclei abundances is studied. In Section 7 we discuss the contribution of SNIa to the production of radiogenic ^{92}Nd, ^{146}Sm and ^{97,98}Tc. Finally, conclusions and work in progress are drawn in Section 8.

2. Type Ia supernova models and tracer particles

We used the SNIa-explosion model (DDT-a) described in detail by TRV11. It is a representative example of the single-degenerate scenario in which the WD has accreted material from a main-sequence or evolved companion star until it finally approaches the Chandrasekhar mass and explodes as a delayed detonation. The model is based on the two-dimensional simulations presented by Kasen et al 2009.

The explosion itself is simulated in 2D by means of the combustion code LEAFS (Reinecke et al. 1999; Reinecke et al. 2002; Röpke 2005; Röpke & Hillebrandt 2005) which follows the evolution with an Eulerian grid. In order to compute for each zone of the star the history of temperature and density over time for each zone of the star we introduce a Lagrangian component in the form of tracer particles. With the tracer-particle method it is possible to reconstruct the ensuing nucleosynthesis. The nuclear post-processing calculations are performed separately for each tracer. Summing the chemical composition over all tracer particles gives the total yields. The tracer particles method was first introduced by Nagataki et al. (1997) for ccSSNe, and by Travaglio et al. (2004b, 2005) for SNIa.

For 2D simulations it has been verified that 51,200 particles as used here, uniformly distributed in mass coordinates, give sufficient resolution (Seitenzahl et al. 2010). For each tracer particle we follow the explosive nucleosynthesis with a detailed nuclear reaction network for all isotopes up to ^{209}Bi. We select tracers within the typical temperature range for p-process production, i.e. $(1.5 - 3.7) \times 10^9$ K, and analyze their behavior in detail, exploring the influence of different s-process seeds on the p-process nucleosynthesis. In order to determine the s-process enrichment prior to the explosion, we assume recurrent flashes occurring in the He-shell during the accretion phase with neutrons mainly released by the ^{13}C(α,n)^{16}O reaction (Iben 1981; TRV11). This applies under the assumption that a small

amount of protons are ingested in the top layers of the He intershell. Protons are captured by the abundant ^{12}C and convert it into ^{13}C via ^{12}C(p,γ)^{13}N($\beta^+\nu$)^{13}C at $T \simeq 1 \times 10^8$ K.

3. *s*-seeds at different metallicities

In our model, *p*-process nucleosynthesis occurs in SNIa starting from a pre-explosion *s*-process enriched seed composition. Therefore, it is essential to determine the *s*-process enrichment prior to the explosion. Here, we assume enhanced *s*-distributions produced directly by a sequence of thermal-pulse instabilities in the accreted material. This idea has been described in detail by TRV11 and was previously discussed by Iben (1981), Iben & Tutukov (1991), and Howard & Meyer (1993).

To be more specific, we assume recurrent flashes to occur in the He-shell during the accretion phase. The matter accumulated onto the carbon-oxygen white dwarf (hereafter CO-WD) therefore becomes enriched in *s*-nuclei. However, the mass involved and the physical properties of the ^{13}C-pocket, providing the free neutrons for the *s*-process, still have to be considered as free parameters. Since no physical models are available we explore different *s*-process distributions in order to better understand the dependence of our results on these initial seeds (see also the discussion in TRV11 and Travaglio et al. 2012).

For the present work we calculate *s*-process distributions for 8 metallicities, i.e. Z =0.02, 0.019, 0.015, 0.012, 0.011, 0.010, 0.006, 0.003 (a refined *s*-seed metallicity grid is necessary for chemical evolution calculations since the *s*-seeds are strongly dependent on metallicity), and we interpolate for all the other metallicities in between in order to calculate Galactic chemical evolution. We also investigate the effect of the *s*-seeds with different ^{13}C-pocket properties (ST×2, ST×1.3, ST, ST/1.5, where $\sim 4 \times 10^{-6} M_\odot$ of ^{13}C in the pocket corresponds to the ST case, Gallino et al. 1998; see Gallino et al. 1998 and Bisterzo

et al. 2010 for a detailed discussion of ^{13}C-pocket profiles). The *s*-process seeds adopted are shown in Figure 1 for the ST×2 ^{13}C-pocket case, and metallicites of Z =0.01, 0.006, 0.004, 0.003. In Figure 2 we show the average of four ^{13}C-pockets at different metallicities. In all figures the s-seed abundances are normalized to the solar abundances of Lodders (2009).

As discussed by Gallino et al. (1998) and Travaglio et al. (1999), the synthesis of heavy nuclei requires neutron captures starting from Fe seeds, so that the *s*-process is expected to decrease with decreasing metallicity, i.e. to be of *secondary* nature. However, the abundances produced depend not only on the initial Fe concentration but also on the neutron exposure. The concentration of ^{13}C in the pocket is of *primary-like* nature (it is built from H and freshly made C, and hence is independent of metallicity), while the abundance of the neutron absorber ^{56}Fe varies linearly with Z. Therefore, for a given amount of ^{13}C in the pocket, the neutron exposure (proportional to the ratio ^{13}C/^{56}Fe) is expected to increase linearly with decreasing metallicity. This dependence would compensate for the secondary nature of the *s*-elements, if the yields of *s*-nuclei were linearly dependent on both neutron exposure and Z. In addition, the behavior of ^{208}Pb has to be considered separately (Travaglio et al. 2001). The gradual increase of the neutron exposure towards low metallicities masks the expected secondary behavior (see also Clayton 1988), resulting in a rather complex dependence of *s*-process yields on metallicity. For the lower metal content the neutron flux feeds Pb (in particular ^{208}Pb). A clear understanding of the *s*-seeds behavior versus metallicity, including the production of neutron-magic ^{208}Pb at the termination of the *s*-process path, is very important for the nature of *p*-process (see Section 4).

Figure 1 shows a variation by a factor of $\simeq$10 for the abundances of the light *s*-only isotopes (up to $A \simeq$140) when Z = varies from 0.003 to 0.01, and a spread of $\simeq$5 for heavy *s*-only nuclei (with $A >$140). For ^{208}Pb, the variation is by a factor of $\simeq$8, but its trend is

inverted with respect the behavior of other s-only isotopes (i.e. lower Z gives higher ^{208}Pb abundance). In Figure 2 we plot the average of four different ^{13}C-pockets (ST×2, ST×1.3, ST, ST/1.5) for the metallicities discussed above. The behavior of the s-only isotopes is different from that seen in Figure 1: still a rough dependence on Z for light s-nuclei in the range $90< A < 120$ is observed, but the variation is now reduced by a factor of 3. The spread is progressively decreasing for higher metallicities. Further on, for heavy s-isotopes with $140 < A \leq 204$, an almost unique and flat distribution is obtained, independent of metallicity with an enhancement around 2000 times solar. Eventually, for ^{208}Pb a spread of about a factor of 4 stands out again, with the lowest metallicity showing the highest ^{208}Pb abundance, at the level of 5000× solar. The general trend sketched above can be understood in the light of the typical s-process enhancement occurring in AGB stars. For a given ^{13}C-pocket strength, decreasing the metallicity the s-flow feeds more and more ^{208}Pb at the termination of the s-path. At the same time a progressive depletion of the lighter s-process isotopes is found up to the magic neutron number $N = 82$ (^{138}Ba to ^{142}Nd). In the region between the magic neutron number nuclei N =82 and N =126, an almost flat s-process production factor ensues. A similar trend occurs at a fixed metallicity by increasing the ^{13}C-pocket strength. We recall here that case STx2 is around the maximum ^{13}C-pocket strength we can reach, beyond which further proton ingestion during a third dredge up episode from the envelope would result in a decrease of ^{13}C and production of the neutron poison ^{14}N (see the review by Busso, Gallino, & Wasserburg 1999). In other words, with decreasing metallicity the otherwise flat s-process distribution near the neutron magic numbers N = 50 amd N = 82, corresponding to atomic mass numbers around A =90 and A =140, and also at the termination of the s-path at around A =208 are progressively distorted.

In Figure 3 we show the s-seeds for the range of ^{13}C-pockets (ST×2, ST×1.3, ST, ST/1.5, ST/2) and metallicities (Z = 0.02, 0.019, 0.015, 0.012, 0.011, 0.010, 0.006, 0.003)

we cover in the Galactic chemical evolution calculations (see Section 6 for discussion).

4. *p*-process at different metallicities

The *p*-process nucleosynthesis is calculated using a nuclear network with 1024 species from neutrons and protons up to ^{209}Bi combined with neutron, proton, and α-induced reactions and their inverse. The code used for this work was originally developed and presented by Thielemann et al. (1996). We employ the nuclear reaction rates based on the experimental values and the Hauser & Feshbach statistical model NON-SMOKER (Rauscher & Thielemann 2000), including the recent experimental results of Maxwellian-averaged neutron capture cross section of various *p*-only isotopes (Dillmann et al. 2010; Marganiec et al. 2010). Theoretical and experimental electron capture and β-decay rates are from Langanke & Martínez-Pinedo (2000).

We discuss in this Section the sensitivity of *p*-process production to *s*-seeds at different metallicites. We analyze the *primary*/*secondary* nature of the resulting *p*-nuclei. According to Rauscher et al. (2013) (and references therein) the *p*-process is of *secondary* nature and scales with the amount of seed nuclei in the star. In this work we present our results obtained with SNIa models which only partly confirm this statement.

In Figure 4 we plot the resulting *p*-process abundances, starting from ^{74}Se, obtained by using different *s*-seeds at different metallicities. On the axis of ordinates the production factor of each isotope is plotted with respect to solar, normalized to ^{56}Fe. Note that the abundances of *p*-nuclei heavier than $A = 100$ are much higher than a factor of $\sim$3 times their solar value. However, in this Figure we plot the nucleosynthesis resulting from one single star and not the integrated abundances over all the Galaxy (see Section 6 for discussion). The choice for these ^{13}C-pockets and metallicities will be used for our best fit

of Galactic chemical evolution calculation.

In order to better understand the dependence of p-nuclei production on metallicity and the ^{13}C-pocket, we show in two separate figures (Figure 5 and Figure 6) the behavior of p-process nucleosynthesis as a function of metallicity and the ^{13}C-pocket, respectively. From Figure 5 we can see that the first three p-only isotopes, ^{74}Se, ^{78}Kr, and ^{84}Sr, show a secondary behavior: their abundances scale almost linearly with Z. They depend mainly (for about 60-70%) on the light (up to $A \simeq$140) s-seeds that, as shown in Figure 1 and Figure 2, are strongly dependent on metallicity. Starting from ^{90}Zr (even if this isotope is not p-only it has to be included in the discussion, see also TRV11) and ^{92}Mo and up to ^{138}Ba, the p-nuclei show a very weak dependence on Z. The isotopes in this atomic mass-number range are mainly produced by photodisintegration from the heavy s-seeds isotopes, thus showing a primary-like behavior (see Figure 6). Isotopes in the region from ^{136}Ce up to ^{196}Hg scale with metallicity but show the opposite trend, i.e. highest abundances for the lowest metallicities. TRV11 (see also Dillmann et al. 2008a) discussed the fact that Pb-seeds are converted to nuclei of lower mass by photodisintegration sequences starting with (γ,n) reactions. Therefore, an important contribution to the heavy p-only isotopes is obtained.

We also found, as discussed in TRV11, that the isotopes ^{113}In, ^{115}Sn, ^{138}La, ^{152}Gd, and ^{180m}Ta, diverge from the average p-process production. Among them, ^{152}Gd and ^{180m}Ta have an important contribution from the s-process in AGB stars (Arlandini et al. 1999), or the neutrino process in ccSN (Woosley et al. 1990; Wanajo et al. 2011). Both ^{113}In and ^{115}Sn are not fed by the p-process nor by the s-process. For these, we refer to the discussion of Dillmann et al. (2008b) and TRV11.

The still puzzling ^{94}Mo deserves special attention. Can nuclear uncertainties account for the low ^{94}Mo yield, compared to the other p nuclei, in our models? Howard et al. (1991)

demonstrated that most of the ^{94}Mo is produced from ^{98}Mo through a (γ,n) chain.

We confirmed that a similar reaction chain also acts in our models. To illustrate this, Figure 8 shows three exemplary trajectories for which time-integrated reaction flows are plotted in Figures 9−11. The flow shown in Figure 9 gives a maximum production of ^{94}Mo (the corresponding trajectory is labeled "^{94}Mo$_{\rm max}$" in Figure 8). The one shown in Figure 10 also favors ^{94}Mo production but at a lower level (the corresponding trajectory is labeled "^{94}Mo$_{\rm drop}$" in Figure 8). In both cases, ^{94}Mo is fed through (γ,n) reaction sequences, with the strongest flow originating at ^{98}Mo, which,in turn, is replenished to some extent also by a small flow originating from ^{100}Mo. It should be noted that the reactivities for this (γ,n) sequence are experimentally well constrained, as they involve stable nuclei and the corresponding (n,γ) reaction cross sections have been measured (Dillmann et al. 2006). Thermal population of excited states does not play a role in these nuclei and thus the measured (n,γ) cross sections allow to compute the (n,γ) and (γ,n) rates without further theory uncertainties (Rauscher 2012, 2014). Therefore this part of the flow does not bear large nuclear uncertainties, it is rather determined by the seed abundances received by the stable Mo isotopes. Some production of ^{94}Mo is also found via ^{95}Tc(γ,p)^{94}Mo. Its contribution to ^{94}Mo, however, is an order of magnitude lower than that of the (γ,n) sequence and thus it does not contribute appreciably to the uncertainty although the ^{94}Mo(p,γ) reactivities are unmeasured.

Consequently, the only significant nuclear uncertainty is found in the destruction of ^{94}Mo by ^{94}Mo(γ,n)^{93}Mo. As already discussed by Travaglio et al. (2014), the sequence ^{94}Mo(γ,n)^{93}Mo(γ,n)^{92}Mo, leads to production of ^{92}Mo, with ^{94}Mo(γ,n)^{93}Mo being the slower, and thus determining, reaction here. A conservative estimate for the uncertainty of this rate (taken from Rauscher & Thielemann 2000) is a factor of 2.

The comparison between the "^{94}Mo$_{\rm max}$" and "^{94}Mo$_{\rm drop}$" trajectories in Figure 8 shows

that "$^{94}\mathrm{Mo}_{\mathrm{drop}}$" reaches a slightly higher peak temperature. This higher temperature not only increases the (γ,n) flow, that destroys ^{94}Mo without increasing the production notably but also enables further destruction of ^{94}Mo by $^{94}\mathrm{Mo}(\gamma,\alpha)^{90}\mathrm{Zr}$. The latter reaction is offset by a slight enhancement in $^{95}\mathrm{Tc}(\gamma,\mathrm{p})^{94}\mathrm{Mo}$ but the flow through this reaction is still lower by a factor of 0.1 than the increased destruction flow. This illustrates that ^{94}Mo can only be produced within a narrow temperature window: at low temperature, the (γ,n) flow is small or non-existent, at too high temperature ^{94}Mo is destroyed by additional reactions. Prerequisite for the efficient production of ^{94}Mo by photodisintegration in any site is that the mainly contributing trajectories spend as much time as possible in this temperature window.

Finally, Figure 11 shows the flows for a trajectory leading to a minimal production of ^{94}Mo although the achieved peak temperature is similar to that in the "$^{94}\mathrm{Mo}_{\mathrm{max}}$" case (the corresponding trajectory is labeled "$^{94}\mathrm{Mo}_{\mathrm{min}}$" in Figure 8; incidentally this is the same trajectory giving a maximum ^{92}Nb production as shown in Figure 5 of Travaglio et al. 2014). Inspection of the flows shows that all (γ,n) flows in this region are significantly suppressed compared to the "$^{94}\mathrm{Mo}_{\mathrm{max}}$" case in Figure 9. The $^{94}\mathrm{Mo}\longrightarrow{}^{93}\mathrm{Mo}$ flow is too small to show in the plotted range. The $^{91}\mathrm{Zr}\longrightarrow{}^{92}\mathrm{Zr}$ flow is even replaced by its reverse. The key to understanding the difference is the fact that the "$^{94}\mathrm{Mo}_{\mathrm{min}}$" trajectory reaches photodisintegration temperatures only at much higher density (note the logarithmic scale of the horizontal axis in Figure 8). At all times, $A(\mathrm{n},\gamma)B$ and $B(\gamma,\mathrm{n})A$ rates are competing. Their relative strengths are on one hand determined by the reaction Q-value (which is given through the well-known nuclear masses) but on the other hand (n,γ) rates also scale with the available neutron density whereas (γ,n) do not (Rauscher 2011). At the temperatures at which photodisintegration of nuclei in the Mo region becomes possible, heavier nuclei are already significantly destroyed because they are less tightly bound (their Q-value for (n,γ) is lower than that of lighter nuclei; see also Rauscher et al. 2013). This allows (n,γ)

reactions to occur in the lighter region and at high density they will be faster than their (γ,n) counterparts. This illustrates the important point that significant production of p-nuclei in a γ-process is possible only when the densities remain limited, i.e. it depends sensitively on the thermodynamic histories of the explosive layers. For example, a model in which more trajectories experience lower densities during γ-processing would lead to increased ^{94}Mo production. However, since this scenario will affect all (n,γ)/(γ,n) ratios and thus it is unclear whether it would lead to an enhancement of the final ^{94}Mo with respect to the other light p-nuclides. This has to be investigated in detail in future calculations because the impact of enhanced (n,γ) rates at higher density is not trivial as it depends on the specific Q-values in the (γ,n) chains producing specific isotopes. Furthermore, it will also impact other reaction types (such as (p,n), (p,γ), and their reverses) in different ways and thus the final outcome strongly depends on the actual reaction sequences producing and destroying a specific nucleus. This may change the ratio of the ^{94}Mo abundance also relative to abundances of other p-nuclei but it remains an open question whether the required relative increase by a factor of 10 can be achieved.

5. The role of s-seeds of different atomic mass number for p-process nucleosynthesis

In order to understand in detail the s-seed origin of each p-nucleus, we performed the following study: fixing the metallicity ($Z = 0.006$, i.e., to a value where we find the highest production of p-nuclei in our Galactic chemical evolution calculations, see Section 6) and fixing a ^{13}C-pocket (i.e., STx2 which is the highest value we used), we first tested the role of the s-seed ^{208}Pb alone, by assigning solar abundances to all other s-seed nuclei. Details of the resulting effect on p-nucleosynthesis are given in Table 1 (third column for the ^{208}Pb only case, and second column for the standard case). A ^{208}Pb seed alone contributes about

30% to ^{74}Se, and 10-20% (or less) to all the other light-p nuclei up to ^{158}Dy (with the exception of ^{144}Sm, where ^{208}Pb alone accounts for about 45%). The contribution to the isotopes between ^{162}Er and ^{190}Pt from ^{208}Pb is about 40%. Finally, for the heaviest of the p-only nuclei, ^{196}Hg, we find the highest share (60%) in production originating from ^{208}Pb.

In Table 2 we list all s-isotopes which we find to have p-contribution. For these isotopes we report in the last column the effect of ^{208}Pb. We find that most of these isotopes (from ^{80}Kr up to ^{176}Hf), the ^{208}Pb seed contributes about 10-20% (or less). A similar analysis has been carried out accounting for either as s-nuclei either the only heavy s-nuclei ($140 \leq A < 208$) or the light s-nuclei ($70 \leq A < 140$) only. The results are shown in Table 1: in Column 6 the results for the heavy s-seed only case and in Column 7 the light s-seed only case are given. Not surprisingly, the heavy s-nuclei are most important for the heavy p-nuclei, in particular for ^{184}Os (100% of contribution), ^{158}Dy (89%), ^{136,138}Ce (about 84% and 75%, respectively), ^{190}Pt (about 73%), and ^{156}Dy (about 70%), but there are also significant contributions of about 40-60% are to the other heavy p-isotopes in the region from ^{144}Sm up to ^{196}Hg. We also find ∼30-40% of the light p-nuclei up to ^{132}Ba to originate from heavy s-seeds, with the exception of ^{94}Mo and ^{130}Ba, which have a lower share of ∼15%. In contrast, light s-seeds are the main producers of the light p-isotopes, and they account for about 73% for ^{74}Se and ^{94}Mo (where important contribution from other stellar sources or errors in reaction rates can be estimated), and finally ^{130}Ba (about 80%). All other light-p isotopes are produced from light-s seeds with typical sharesin the rage from 40 to 60%. The heaviest p-nuclei are almost unaffected by the light-s seeds.

In the fourth columns of Table 1 and Table 2 we show results of a second test for comparison, where we retain a metallicity of $Z = 0.006$, but reduce the strenght of the ^{13}C-pocket by using the STx1.3 model. For this case we test the role of ^{208}Pb seed for p-process nucleosynthesis, as we did in the above standard case (see fifth column in Tables

1, 2). Comparing the two cases presented in Table 1 (column 3 and 5), we notice that typically the case with STx2 ^{13}C-pocket and a ^{208}Pb seed contributes by a factor of $\sim$2 to the light-p nuclei with respect to the case STx1.3 ^{13}C-pocket and ^{208}Pb seed. For the abundance of ^{144}Sm we obtain identical results for STx2 and STx1.3 cases. In contrast, however, we observe an increased production of the heavy-p nuclei for the case STx2 and ^{208}Pb seed by $\sim$10%. The only exception is for the heaviest p-nucleus ^{196}Hg, where we find a highest abundance in the case STx1.3 ^{208}Pb alone. The reason for this behavior is that at the same metallicity ($Z = 0.006$) the ^{13}C-pocket STx1.3 is less efficient than the ^{13}C-pocket STx2 for the production of heavy-s as well as for ^{208}Pb.

6. Galactic chemical evolution

The main goal of this work is to provide predictions for Galactic chemical evolution of p-nuclei. For this, we employ the Galactic chemical evolution code presented by Travaglio et al. 1999, 2001, 2004. The model considers the Galaxy as the evolution of three interconnected zones, halo, thick disk and thin disk. The matrix of the isotopes within the chemical evolution code was set to cover all the light nuclei up to the Fe-group, and all the heavy nuclei along the s-process path up to ^{209}Bi. For the present work we extended the matrix of the isotopes to account for the p-nuclei and we followed their evolution over time/metallicity until solar metallicity was reached. We included in the code the p-nuclei abundances obtained from our SNIa model at various metallicities as discussed in Section 4, and interpolate between them smoothly. In Figure 7 we show the resulting p-process production factors taken at the epoch of Solar System formation for nuclei in the atomic mass number range $70 \leq A \leq 210$. To be more clear we note that for these results we only include SNIa for the contribution to p-nuclei. Our choice for the s-seeds was introduced in Section 3 (see Figure 3). As discussed in the previous section, it is clear that a few nuclei

originally ascribed to the p-only group (^{113}In, ^{115}Sn, ^{138}La, ^{152}Gd, and ^{180m}Ta) are far below the average of the other p-nuclei. Thus, if this model is correct, they should be ascribed to different astrophysical sources. As shown in Figure 7 and detailed in Table 3, we find in our Galactic chemical evolution calculations that all the other p-only isotopes are—within a factor of about three—produced at the Solar System composition. The lightest p-nucleus ^{78}Kr and the heaviest ^{158}Dy and ^{180}W can be ascribed to the same production site when an additional uncertainty factor of two is included (which seems reasonable given the large uncertainties in photodisintegration rates). Therefore, for the first time, we are able to explain the synthesis of almost all p-isotopes production in one single scenario. The most striking problem we face is the very low relative abundance of the true p-only ^{94}Mo with respect the the average of all other p-only nuclei, which is possibly related to the theoretical estimate of the neutron capture on unstable ^{93}Mo. The effect of the nuclear uncertainties will be explored in a forthcoming paper.

Figure 7 and Table 4 also show that neutron magic ^{90}Zr and especially ^{96}Zr receive an important contribution by the p-process (about 20% and 40%, respectively). Moreover, it is not excluded that the most proton-rich s-only isotopes for a given element may receive some contribution from the p-process. As illustrated in Figure 7, this is the case for ^{80}Kr and ^{86}Sr, with p-contribution of the order of 10%. However, before examining the problem in more detail, an analysis of the uncertainties in the involved reaction rates is necessary. Out of the light p-nuclei the isotopes ^{78}Kr, ^{94}Mo, ^{108}Cd, and ^{114}Sn are by a factor of three or more (for ^{94}Mo) less abundant compared to the solar value. Among the heavy-p nuclei ^{158}Dy is also by more than a factor of three below the solar abundance. In contrast, we found ^{180}W higher by a factor of more than three with respect to solar. Under the hypothesis that SNIa are responsible for 2/3 of solar ^{56}Fe, and assuming that our DDT-a model represents the typical SNIa with a frequency of 70% (Li et al. 2011), we conclude that they are responsible for at least 50% of all p-nuclei.

With the same approach, Travaglio et al. (2014) discussed the origin of the short-lived radionuclides ^{92}Nb and ^{146}Sm. They compared the value of the ratio between the abundances of these radionuclides and those of the corresponding stable reference isotopes ^{92}Mo and ^{144}Sm to what has been recently measured in meteorites (Rauscher et al. 2013). The conclusion is that SNIa can also play a key role in the production of ^{92}Nb and ^{146}Sm, but nuclear uncertainties have to be taken into account.

In the framework of Galactic chemical evolution of p-nuclei, the role of ccSN has also to be taken into account. Rauscher et al. (2002) followed the γ-process through the presupernova stages and the supernova explosion. As expected for the weak s-process component in massive stars, only s-nuclei in the mass range $64 \leq A \leq 88$ are produced and occurred in situ prior to the explosion phase. Rauscher et al. (2002) presented results for 15, 19, 21, 25 $M_{\odot}$ ccSNe modeled in spherical symmetry and with initial solar metallicity. For the 15, 21, and 25 $M_{\odot}$ models, proton-rich heavy isotopes in the mass ranges $124 \leq A \leq 150$ and $168 \leq A \leq 200$ were produced in solar abundance ratios within about a factor of two relative to ^{16}O, the most abundant nucleus in the ejecta of ccSNe. For mass numbers $A \leq 124$ and $150 \leq A \leq 165$ the production of the p-isotopes is down by about a factor of $3 - 4$. While the main γ-process synthesizes p-nuclei through photodisintegration reactions during the SN shockfront passage, some of the models showed pre-explosive p-production due to a high entropy in the O/Ne shell of the evolved star. Most of this is wiped out again when the supernova shock sweeps through the layer. Nevertheless, depending on the adopted convection model (see also Bazan & Arnett 1994), some light, strongly bound p-nuclei may survive from pre-explosive production. This behavior complicates predictions for the contribution of ccSNe to the solar composition of p-nuclei. In addition, it has to be taken into account that the SNIa scenario discussed here may not explain all normal events. Thus, alternative scenarios for p-process nucleosynthesis in binary systems should be explored, such as SNeIa from WD-WD mergers (e.g. Pakmor et al. 2010, 2012) or double

detonations in sub-Chandrasekhar mass WDs (e.g. Fink et al. 2010).

7. Conclusions

We have presented results of detailed p-process nucleosynthesis calculations for two-dimensional models of delayed detonations in Chandrasekhar-mass WDs resulting from the single degenerate progenitor scenario. In these SNIa models, the nucleosynthesis was followed by the tracer-particles method. The initial s-seeds were assumed to be created during the mass accretion phase. Since up to now no nucleosynthesis calculations of the accretion phase are available our hypothesis is based on the assumption that a small amount of protons are ingested at the top layers of the He intershell. Following the work of TRV11 on the nucleosynthesis for a solar metallicity SNIa model in the same scenario, we tested and discussed the consequences of different amounts of ^{13}C and different metallicites on the synthesis of p-nuclei. We demonstrated that the ^{208}Pb s-seed alone plays an important role for p-nuclei production, due to photodisintegration chains starting from the heaviest nuclei and going down in mass number. We analyzed the dependence of all the p-isotopes on metallicity, and we identified the isotopes with a weak (like ^{92}Mo and ^{138}Ba) and a strong (in particular the lightest p-isotopes, ^{74}Se, ^{76}Kr, and ^{84}Sr) dependence on Z.

We discussed the still puzzling origin of ^{94}Mo. Clearly, nuclear uncertainties cannot account for the factor of 10 deficiency in ^{94}Mo abundance relative to other p-abundances. The ^{94}Mo production was found to depend on the seeds in the Mo isotopes as well as on the density at which the photodisintegration process occurs. This leaves room for possible variations in the hydrodynamic history of the mainly contributing explosive trajectories which could change the relative p-abundances.

By means of a simple Galactic chemical evolution code, including p-process

contributions at different metallicities, we explored the SNIa contribution to the p-nuclei abundances in the Solar System. We concluded that p-nuclei are mainly of primary-like origin, and that SNIa can contribute at least 50% to the solar abundance of all p-nuclei provided that they result from standard Chandrasekhar-mass delayed-detonations forming in the single-degenerate progenitor channel. Thus we identified a stellar source which, in principle, is able to produce light and heavy p-nuclei almost at the same level relative to ^{56}Fe, including the much debated neutron magic ^{92}Mo and ^{96,98}Ru.

The important contribution from p-process nucleosynthesis to the s-only nuclei ^{80}Kr, ^{86}Sr, and to the neutron magic ^{90}Zr has also been elaborated. Another relevant contribution is to the neutron rich ^{96}Zr, due to neutron captures from the residual abundance of ^{22}Ne during the explosive phase. With our Galactic chemical evolution calculations, it was possible to predict a significant contribution from SNIa in the considered scenario to the extinct p-radionuclides ^{92}Nb, ^{146}Sm, and ^{96,98}Tc in the early Solar System as shown in Travaglio et al. 2014. Alternative scenarios for p-process nucleosynthesis in binary systems have to be taken into account, such as SNeIa from WD-WD mergers, where we also expect some p-process production. A detailed analysis of different SNIa progenitors will be explored in a future work.

This work has been supported by B2FH Association. The numerical calculations have been also supported by Regione Lombardia and CILEA Consortium through a LISA Initiative (Laboratory for Interdisciplinary Advanced Simulation) 2010 grant. C.T. thanks C. Arlandini, P. Dagna, and R. Casalegno for technical support in the simulations. C.T thanks the University of Washington (Institute for Nuclear Theory, Seattle, WA, INT Program INT-14-2b) for the kind support in the last phase of this work. The work of FKR was supported by the Deutsche Forschungsgemeinschaft via the Emmy Noether Program (RO 3676/1-1) and the graduate school "Theoretical Astrophysics and Particle Physics" at

the University of Würzburg (GRK 1147) Additional funding was provided by the ARCHES prize of the German Ministry of Education and Research (BMBF) and the DAAD/Go8 German-Australian exchange program. TR is partially supported by the Swiss NSF, the European Research Council (grant GA 321263-FISH). WH's work was supported by the Transregional Collaborative Research Centre TRR33 "The Dark Universe" und the Cluster of Excellence "Origin and Structure of the Universe" at Munich Technical University.

REFERENCES

Arlandini, C., Käppeler, F., Wisshak, K., Gallino, R., Lugaro, M., Busso, M., & Straniero, O. 1999, ApJ, 525, 886

Arnould, M. 1976, A&A, 46, 117

Arnould, M., & Goriely, S. 2006, Nucl. Phys. A, 777, 157

Audouze, J., & Truran, J.W. 1975, ApJ, 202, 204

Bazan, G. & Arnett, D. 1994, ApJ, 433, L41

Bisterzo, S., Gallino, R., Straniero, O., Cristallo, S., & Käppeler, F. 2010, MNRAS, 404, 1529

Burbidge, E.M., Burbidge, G.R., Fowler, W.A., & Hoyle, F. 1957, Rev. Mod. Phys., 29, 547

Busso, M., Gallino, R., & Wasserburg, G. J. 1999, Annu. Rev. Astron. Astrophys, 37, 239

Cameron, A.G.W. 1957, AJ, 62, 9

Clayton, D.D. 1988, MNRAS, 234, 1

Dillmann, I., Heil, M., Käppeler, F., Plag, R., Rauscher, T., & Thielemann, F.-K. 2006, AIP Conf. Proc. 819, 123; KADoNiS (Karlsruhe Database of Nucleosynthesis in Stars) v0.2, available at `http://www.kadonis.org`

Dillmann, I., Plag, R., Domingo-Pardo, C., Heil, M., Käppeler, F., Rauscher, T., & Thielemann, F.-K. 2008a, Proceedings "International Conference on Nuclear Data for Science and Technology 2007", Nice/ France

Dillmann, I., Rauscher, T., Heil, M., Käppeler, F., Rapp, W., & Thielemann, F.-K. 2008b, Journal of Physics G: Nuclear and Particle Physics, 35, 014029

Dillmann, I., Domingo-Pardo, C., Heil, M., Käppeler, F., Walter, S., Dababneh, S., Rauscher, T., & Thielemann, F.-K. 2010, Phys. Rev. C 81, 015801

Fink, M., Röpke, F.K., Hillebrandt, W., Seitenzahl, I.R., Sim, S.A., & Kromer, M. 2010, A&A, 514, 53

Gallino, R., Arlandini, C., Busso, M., Lugaro, M., Travaglio, C., Straniero, O., Chieffi, A., & Limongi, M. 1998, ApJ, 497, 388

Goriely, S., José, J., Hernanz, M., Rayet, M., & Arnould, M. 2002, A&A, 383, L27

Goriely, S., García-Senz, D., Bravo, E., & José, J. 2005, A&A, 444, L1

Hansen, C.J., Andersen, A.C., & Christlieb, N. 2014, A&A, 568, 47

Howard, W.M., Mathews, G.J., Takahashi, K., & Ward, R.A. 1986, ApJ, 309, 633

Howard, W.M., Meyer, B.S., & Woosley, S.E. 1991, ApJ, 373, L5

Howard, W.M., & Meyer, B.S. 1993, in Proceedings of the 2nd International Symposium on Nuclear Astrophysics, held at Karlsruhe, Germany. Ed. by F. Kaeppeler and K. Wisshak, (Bristol: IOP Publishing) p.575

Iben, I.Jr. 1981, ApJ, 243, 987

Iben, I.Jr., & Tutukov, A.V. 1991, ApJ, 370, 615

Kasen, D., Röpke, F.K., & Woosley, S.E. 2009, Nature, 460, 869

Kusakabe, M., Iwamoto, N., & Nomoto, K. 2011, ApJ, 726, 25

Langanke, K., & Martínez-Pinedo, G. 2000, Nucl. Phys. A, 673, 481

Li, W., et al. 2011, MNRAS, 412, 1441

Lodders, K. 2009, ApJ, 591, 1220

Marganiec, J., Dillmann, I., Domingo Pardo, C., Käppeler, F., & Walter, S. 2010, Phys. Rev. C 82, 035806

Nagataki, S., Hashimoto, N.A., Sato, K., & Yamada, S. 1997, ApJ, 486, 1026

Nomoto, K., Thielemann, F.-K., & Yokoi, K. 1984, ApJ, 286, 644

Pakmor, R., Kromer, M., Röpke, F.K., Sim, S.A., Ruiter, A.J., & Hillebrandt, W. 2010, Nature, 463, 61

Pakmor, R., Edelmann, P., Röpke, F.K., Hillebrandt, W. 2012, MNRAS, 424, 2222

Peterson, R.C. 2013, ApJ, 768, L13

Rauscher, T. 2011, Int. J. Mod. Phys. E 20, 1071

Rauscher, T. 2012, ApJ, 755, L10

Rauscher, T. 2013, Physical Review Letters, 111, 061104

Rauscher, T. 2014, AIP Advances 4, 041012

Rauscher, T., & Thielemann, F.-K. 2000, Atomic Data Nucl. Data Tables, 75, 1

Rauscher, T., Heger, A., Hoffmann, R.D., & Woosley, S.E. 2002, ApJ, 576, 323

Rauscher, T., Dauphas, N., Dillmann, I., Fröhlich, C., Fülöp, Z., & Gyürky, G. 2013, Rep. Prog. Phys., 76, 66201

Reinecke, M., Hillebrandt, W., Niemeyer, J.C., Klein, R., & Gröbl, A. 1999, A&A, 347, 724

Reinecke, M., Hillebrandt, W., & Niemeyer, J. C. 2005, A&A, 386, 936

öpke, F.K. 2005, A&A, 432, 969

öpke, F.K., & Hillebrandt, W. 2005, A&A, 431, 635

Seitenzahl, I.R., Röpke, F.K., Fink, M., & Pakmor, R. 2010, MNRAS, 407, 229

Thielemann, F.-K., Nomoto, K., & Hashimoto, M. 1996, ApJ, 460, 408

Travaglio, C., Galli, D., Gallino, R., Busso, M., Ferrini, F., & Straniero, O. 1999, ApJ, 521, 691

Travaglio, C., Gallino, R., Busso, M., & Gratton, R. 2001, ApJ, 549, L346

Travaglio, C., Gallino, R., Arnone, E., Cowan, J., Jordan, F., & Sneden, C. 2004, ApJ, 601, 864

Travaglio, C., Hillebrandt, W., Reinecke, M., & Thielemann, F.-K. 2004b, A&A, 425, 1029

Travaglio, C., Hillebrandt, W., & Reinecke, M. 2005, A&A, 443, 1007

Travaglio, C., Röpke, F.K., Gallino, R., & Hillebrandt, W. 2011, ApJ, 739, 93

Travaglio, C., Gallino, R., Hillebrandt, W., & Röpke, F.K. 2012, Proceedings of Science, 45

Travaglio, C., Gallino, R., Rauscher, T., Dauphas, N., Röpke, F.K., & Hillebrandt, W. 2014, ApJ, in press

Wanajo, S., Janka, H.-T., & Müller, B. 2011, ApJ, 726, L15

Woosley, S.E., & Howard, W.M. 1990, ApJ, 354, L21

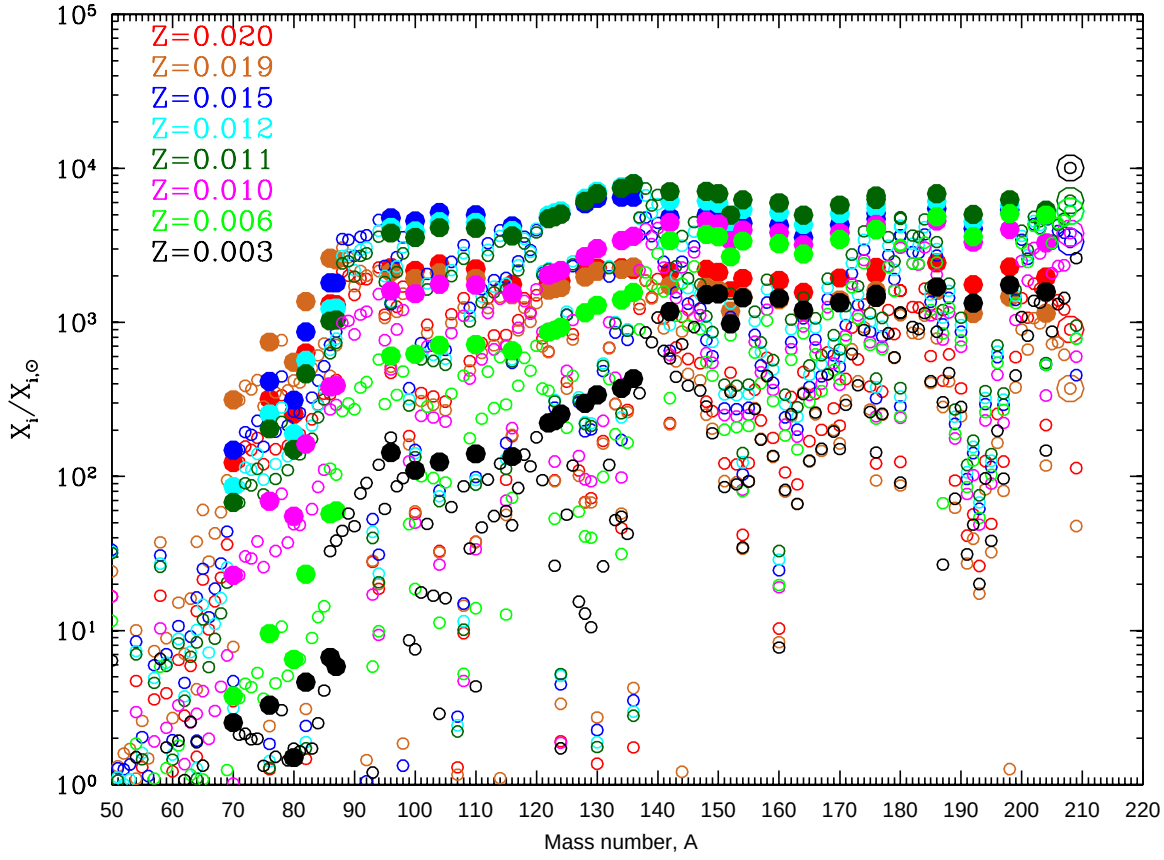

Fig. 1.— Different *s*-seed production factors relative to solar for the ST×2 ^{13}C-pocket and $Z = 0.02$ (*red*), $Z = 0.019$ (*brown*), $Z = 0.015$ (*blue*), $Z = 0.012$ (*cyan*), $Z = 0.011$ (*dark green*), $Z = 0.01$ (*magenta*), $Z = 0.006$ (*light green*), and $Z = 0.003$ (*black*). Filled dots are for *s*-only isotopes. The *big open dot* is for ^{208}Pb, see text for discussion. The solar values for this figure and all other figures of this paper are from Lodders 2009.

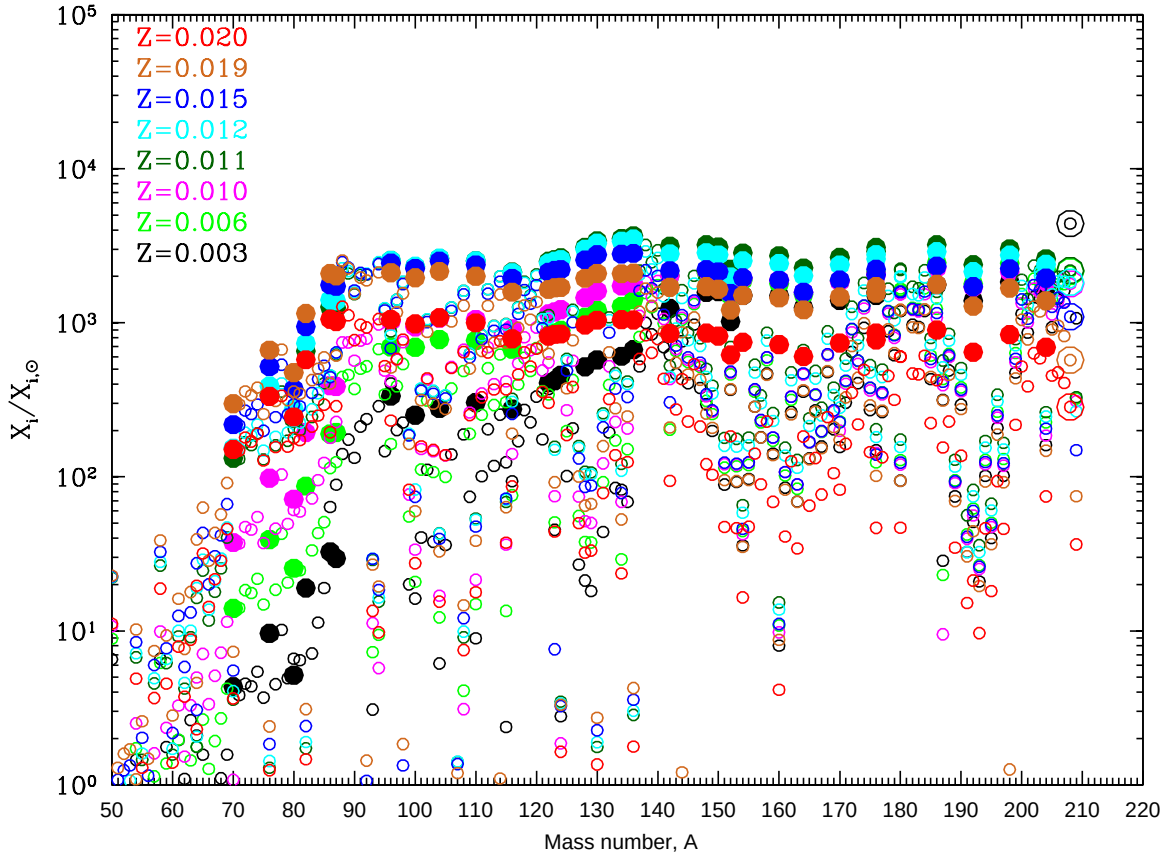

Fig. 2.— Different *s*-seed production factors relative to solar for an average of four different ^{13}C-pockets (ST×2, ST×1.3, ST, ST/1.5 see text for discussion). Colours and symbols used are the same of Figure 1.

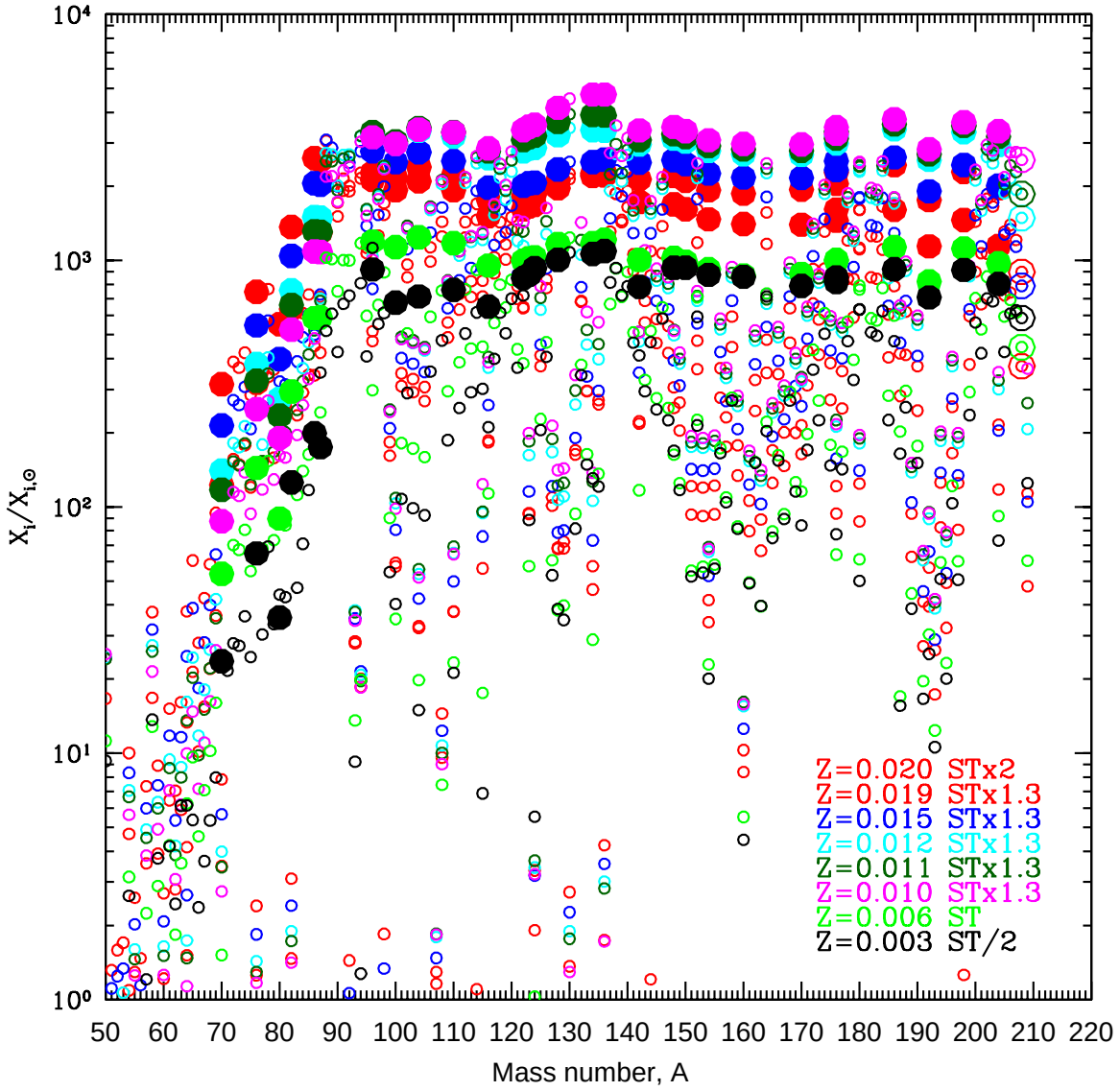

Fig. 3.— Distribution of *s*-seed abundances relative to solar for all ^{13}C-pockets cases and metallicities covered, used for our Galactic chemical evolution calculation. Colours and symbols are the same of Figure 1. See text for a detailed discussion.

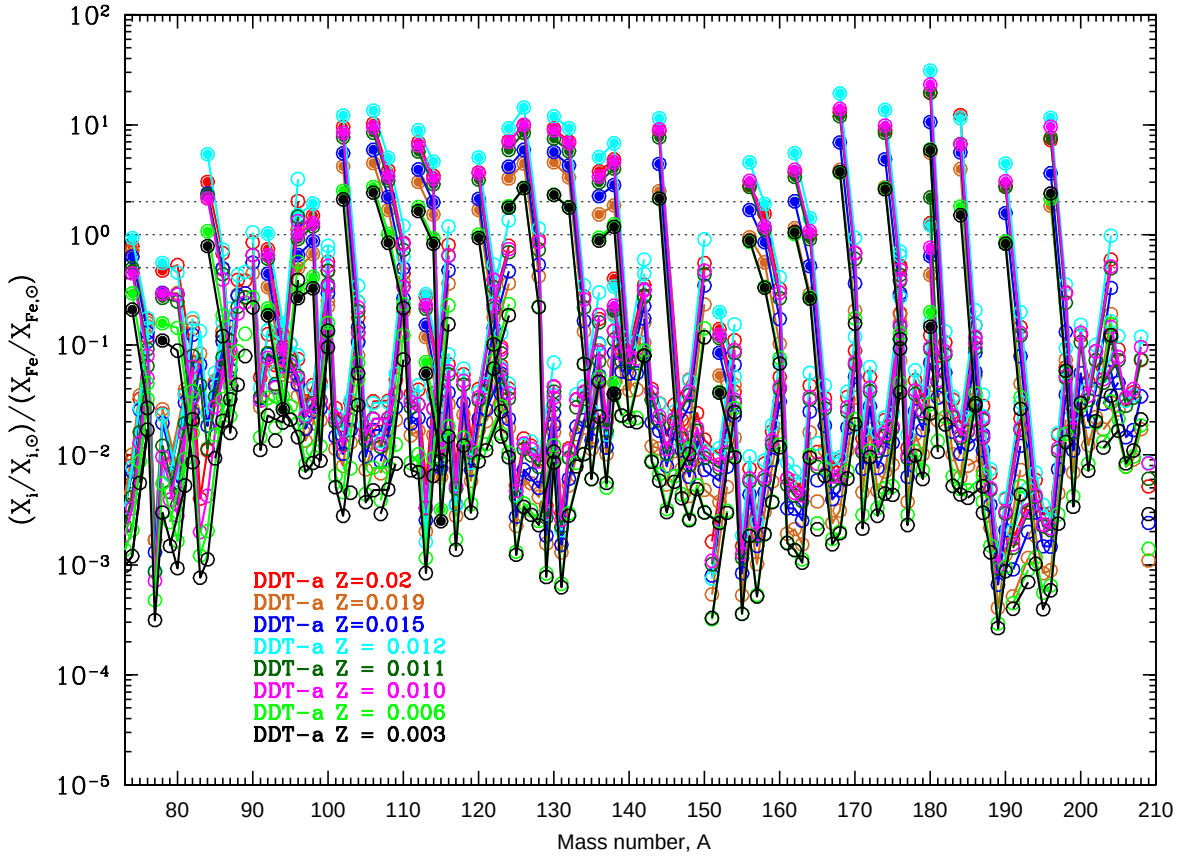

Fig. 4.— p-process yields normalized to solar and to Fe, obtained by using 51,200 tracer particles in the two-dimensional DDT-a model, different metallicities combined with their choosen ^{13}C-pockets. Colours are the same of Figure 1. Filled dots are for p-only isotopes.

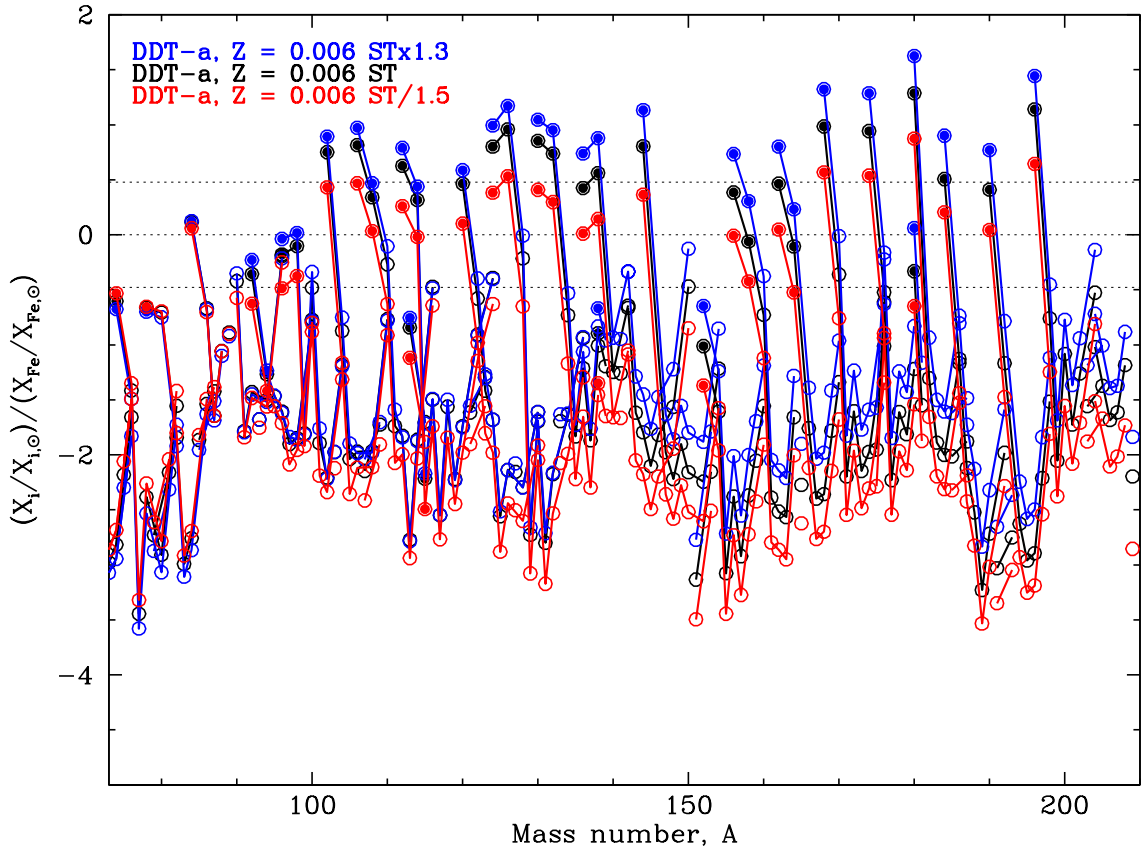

Fig. 5.— p-process yields normalized to solar and to Fe, obtained using 51,200 tracer particles in the two-dimensional DDT-a model, with a fixed metallicity (Z =0.006) and changing ^{13}C-pocket abundance.

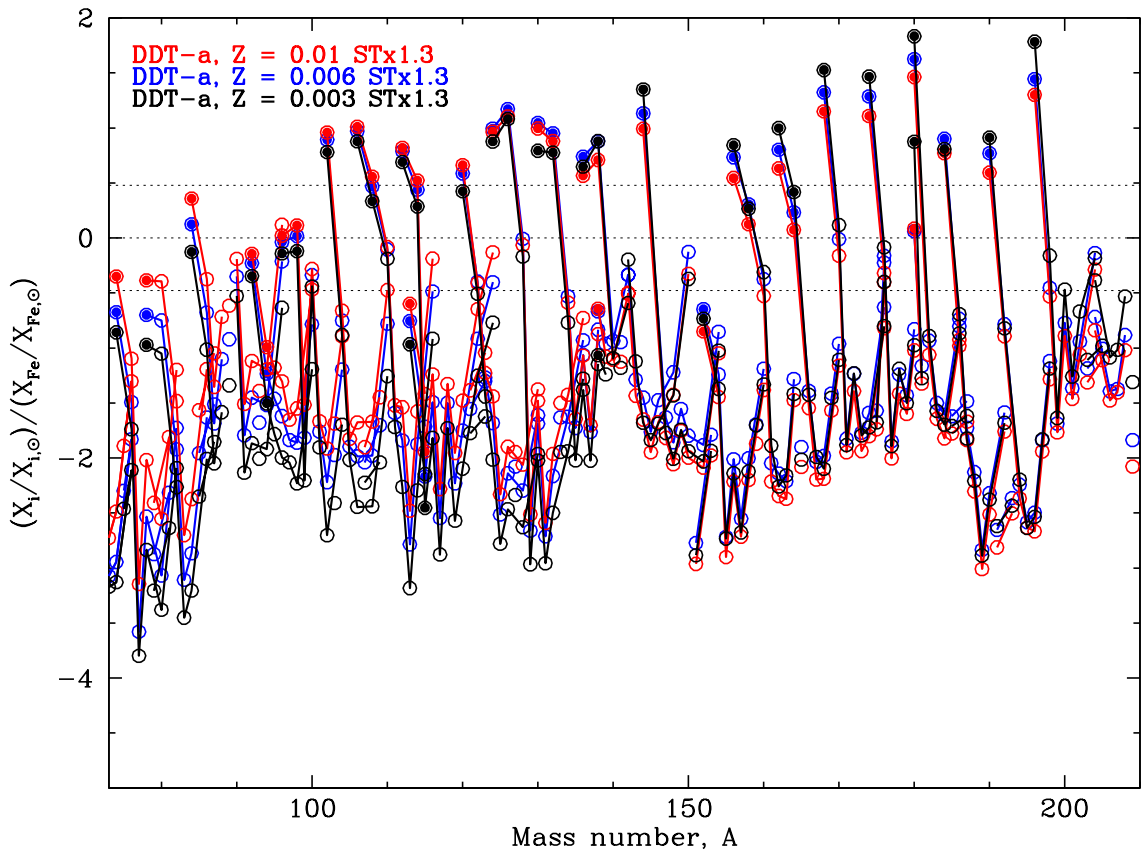

Fig. 6.— The same as Figure 5, but for this figure we fixed the ^{13}C-pocket abundances (ST×1.3) and changed the metallicity.

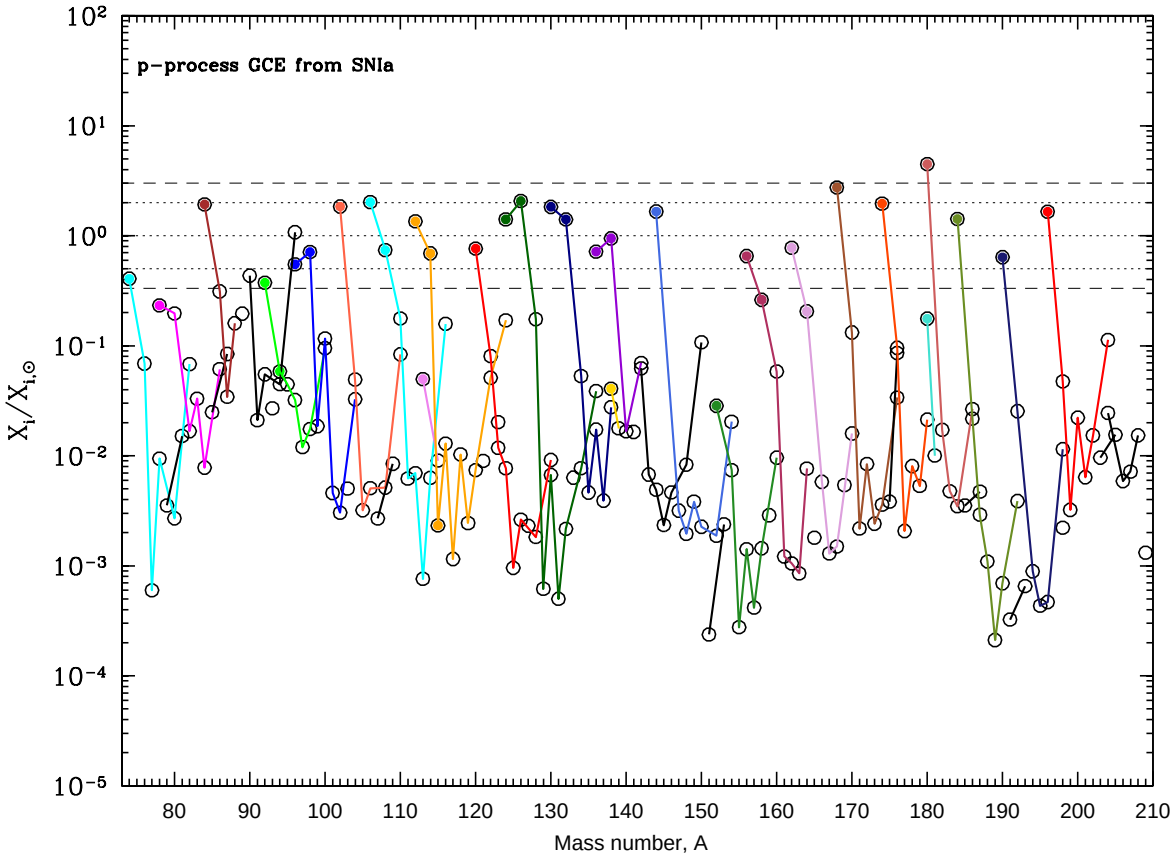

Fig. 7.— Galactic chemical evolution of the *p*-process taken at the epoch of Solar System formation. Filled dots are for the 35 isotopes classicaly defined as *p*-only. The isotopes of each element are connected by a line, and for each element we adopt a different colour. For the *s*-seeds we used the abundances shown in Figure 3 and discussion in the text.

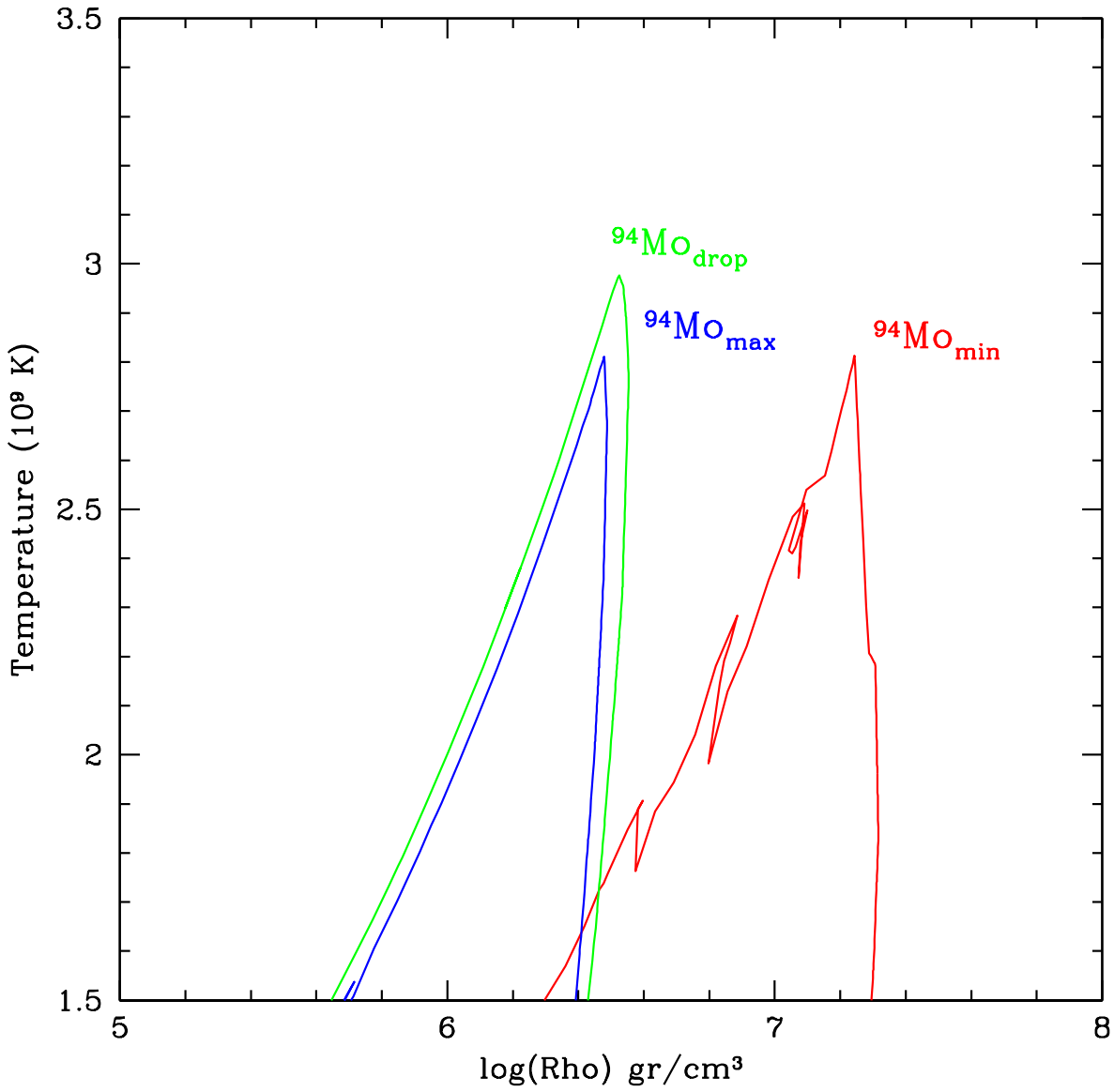

Fig. 8.— Temperature vs density for three different tracers relevant for ^{94}Mo production (see text for details).

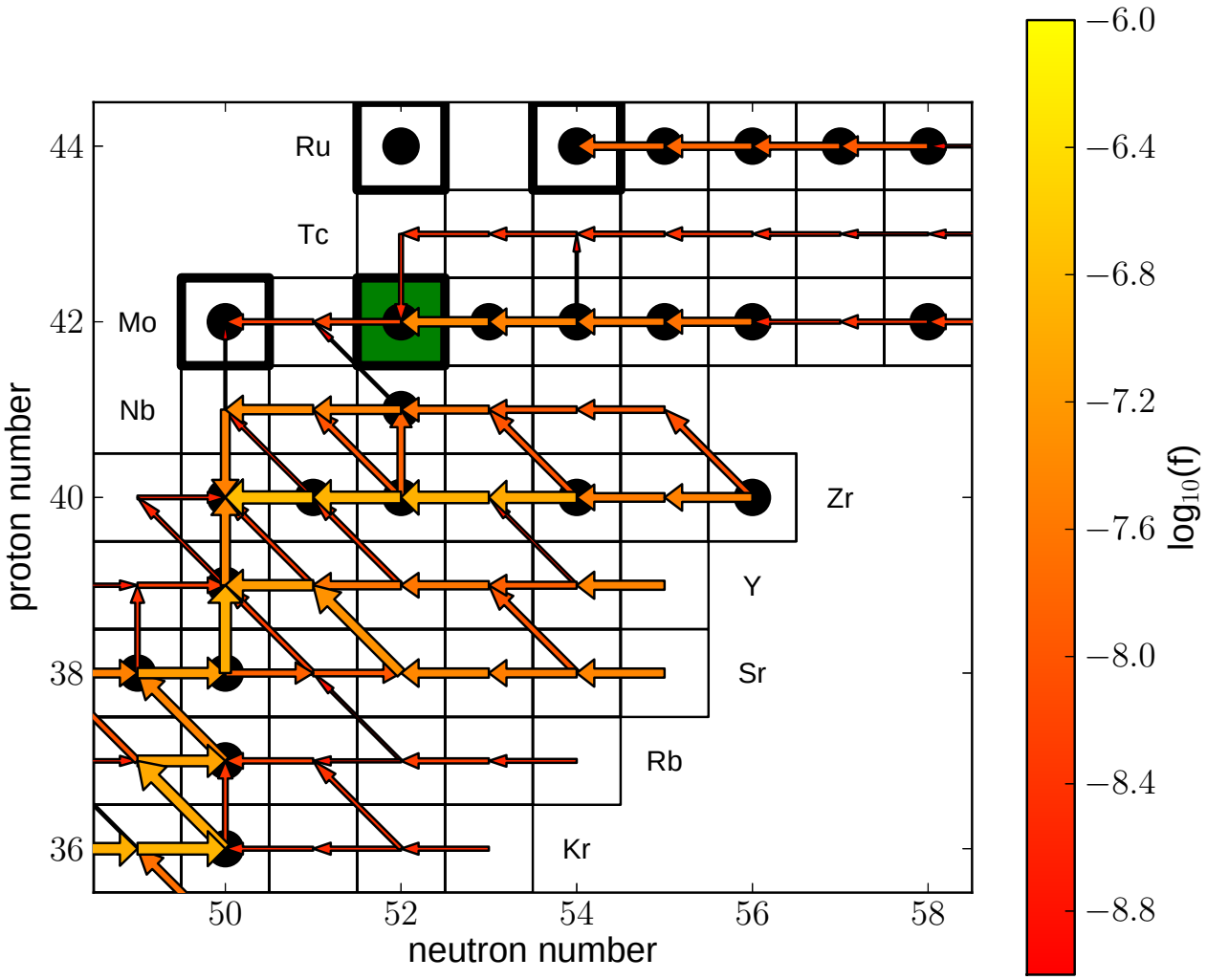

Fig. 9.— Reaction flow for maximum ^{94}Mo production (trajectory $^{94}\mathrm{Mo}_{\mathrm{max}}$ in Fig. 8); size and color of the arrows relate to the magnitude of the time-integrated flux on a logarithmic scale. Only flows down to a factor 0.001 of the maximum flow are shown.

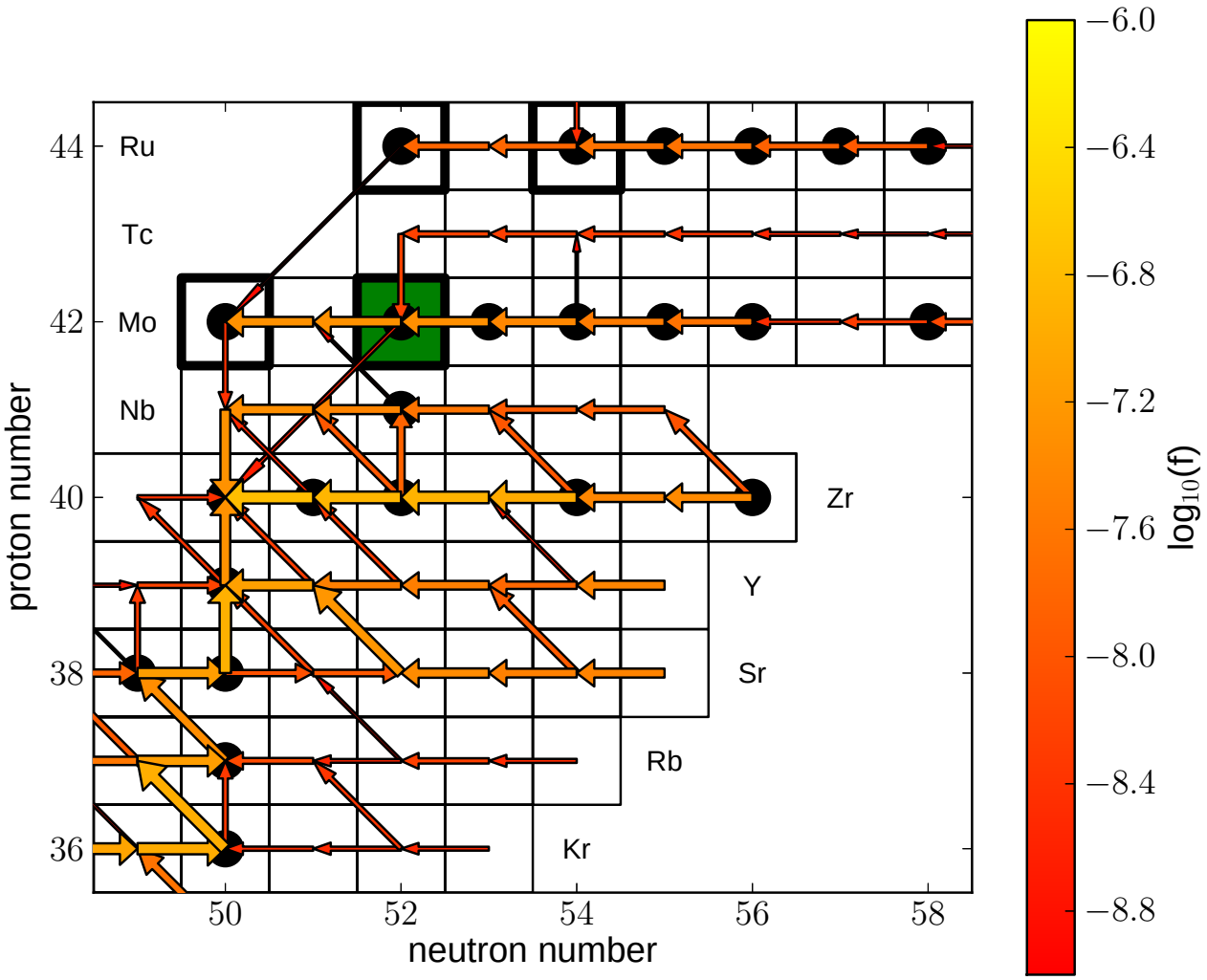

Fig. 10.— Reaction flow for maximum ^{94}Mo production beyond the dropping edge (trajectory $^{94}\mathrm{Mo}_{\mathrm{drop}}$ in Fig. 8); size and color of the arrows relate to the magnitude of the time-integrated flux on a logarithmic scale. Only flows down to a factor 0.001 of the maximum flow are shown.

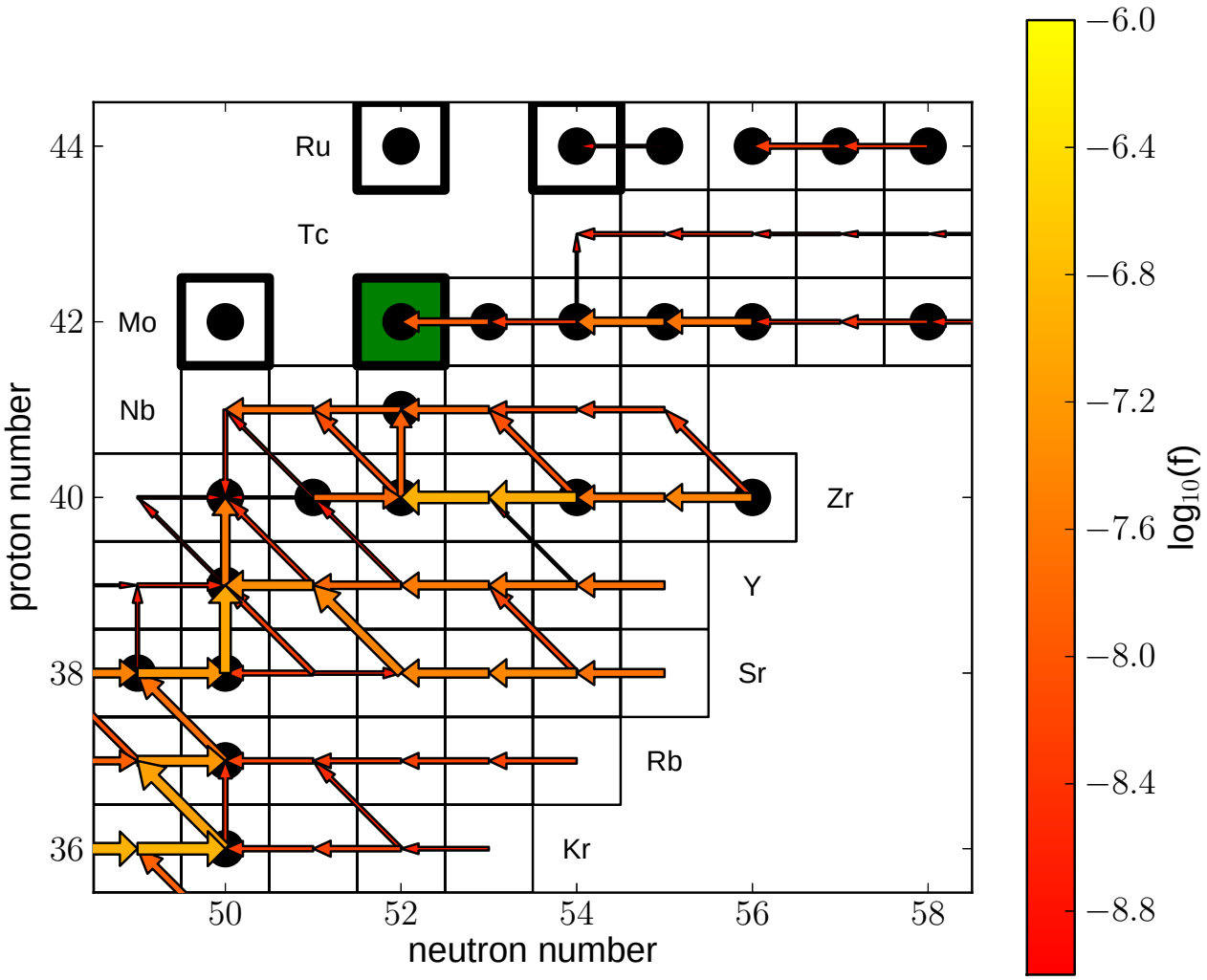

Fig. 11.— Reaction flow for a ^{94}Mo production minimum (trajectory $^{94}\mathrm{Mo}_{\mathrm{min}}$ in Fig. 8); size and color of the arrows relate to the magnitude of the time-integrated flux on a logarithmic scale. Only flows down to a factor 0.001 of the maximum flow are shown.

Table 1. p-nuclides $Z = 0.006$

Isotope	STx2 [(a)]	only ^{208}Pb (STx2) (%)	STx1.3 [(a)]	only ^{208}Pb (STx1.3) (%)	only heavy-s (STx2) (%)	only light-s (STx2) (%)
^{74}Se	5.9766D-08	32	7.7692D-08	22	37	73
^{78}Kr	2.2814D-08	14	2.6779D-08	5	22	60
^{84}Sr	1.6684D-07	15	1.7652D-07	5	24	63
^{92}Mo	3.3110D-07	20	2.5454D-07	10	33	46
^{94}Mo	1.5926D-08	10	1.5816D-08	4	16	74
^{96}Ru	1.5192D-07	22	1.1276D-07	11	35	44
^{98}Ru	5.6763D-08	20	4.4197D-08	10	33	49
^{102}Pd	1.9007D-07	21	1.4257D-07	11	35	45
^{106}Cd	3.4325D-07	22	2.5156D-07	11	37	43
^{108}Cd	7.3755D-08	19	5.7087D-08	10	33	49
^{*113}In	2.3632D-09	14	1.9788D-09	6	24	59
^{112}Sn	4.4177D-07	21	3.2332D-07	11	36	43
^{114}Sn	1.2393D-07	17	9.9142D-08	8	30	54
^{*115}Sn	1.3516D-10	8	1.2630D-10	3	14	75
^{120}Te	3.0791D-08	15	2.5063D-08	7	28	56
^{124}Xe	1.1681D-07	18	8.7859D-08	9	36	45
^{126}Xe	1.6423D-07	20	1.1991D-07	10	40	40
^{130}Ba	9.3644D-08	6	8.6408D-08	2	14	79
^{132}Ba	8.2042D-08	12	6.7356D-08	6	32	56
^{*138}La	1.5568D-10	-	1.5268D-10	-	-	99
^{136}Ce	2.9490D-08	16	2.0296D-08	9	84	-
^{138}Ce	6.1838D-08	25	3.7265D-08	16	75	-
^{144}Sm	4.7213D-07	44	1.9701D-07	40	54	-
^{*152}Gd	4.2205D-10	6	2.8463D-10	3	94	-
^{156}Dy	4.5886D-09	29	2.3545D-09	22	71	-
^{158}Dy	2.4326D-09	11	1.5200D-09	7	89	-
^{162}Er	1.0113D-08	39	4.5391D-09	33	61	-
^{*164}Er	3.2957D-08	40	1.4267D-08	35	59	-
^{168}Yb	3.2922D-08	40	1.4330D-08	34	60	-
^{174}Hf	2.3801D-08	37	1.0562D-08	31	63	-

Table 1—Continued

Isotope	STx2 [a]	only ^{208}Pb (STx2) (%)	STx1.3 [a]	only ^{208}Pb (STx1.3) (%)	only heavy-s (STx2) (%)	only light-s (STx2) (%)
^{*180}Ta	1.0371D-11	-	6.4666D-12	-	100	-
^{180}W	3.9411D-08	40	1.6578D-08	36	60	-
^{184}Os	3.8775D-09	-	2.2520D-09	-	100	-
^{190}Pt	5.2488D-09	27	2.3916D-09	23	73	-
^{196}Hg	9.9030D-08	58	3.5696D-08	61	41	-

[a] – Nucleosynthesis yields.

[*] – Isotopes pointed with * have to be excluded from the p-only list, as discussed by TRV11.

Table 2. s-nuclides with important p-contribution, Z =0.006

Isotope	STx2[a]	only ^{208}Pb (STx2) (%)	STx1.3[a]	only ^{208}Pb (STx1.3) (%)	only heavy-s (STx2) (%)	only light-s (STx2) (%)
^{80}Kr	1.2508D-07	12	1.5196D-07	4	19	58
^{86}Sr	4.2708D-07	13	4.8676D-07	4	20	67
^{90}Zr	3.2537D-06	17	2.8889D-06	7	28	55
^{96}Zr	1.6979D-07	-	2.2666D-07	-	-	100

[a] – Nucleosynthesis yields.

[*] – Isotopes pointed with * have to be excluded from the p-only list, as discussed by TRV11.

Table 3. Galactic chemical evolution of p-nuclides

Isotope	GCE	(GCE/Solar)
^{74}Se	4.186D-10	0.41
^{78}Kr	9.968D-11	0.23
^{84}Sr	5.760D-10	1.93
^{92}Mo	3.643D-10	0.37
^{94}Mo	3.663D-11	0.06
^{96}Ru	1.431D-10	0.55
^{98}Ru	6.294D-11	0.71
^{102}Pd	7.251D-11	1.84
^{106}Cd	1.173D-10	2.02
^{108}Cd	3.067D-11	0.74
^{*113}In	1.232D-12	0.05
^{112}Sn	1.451D-10	1.35
^{114}Sn	5.177D-11	0.69
^{*115}Sn	8.794D-14	0.002
^{120}Te	1.254D-11	0.76
^{124}Xe	3.350D-11	1.41
^{126}Xe	4.281D-11	2.07
^{130}Ba	3.186D-11	1.83
^{132}Ba	2.364D-11	1.40
^{*138}La	5.825D-14	0.04
^{136}Ce	5.816D-12	0.72
^{138}Ce	1.045D-11	0.95
^{144}Sm	5.238D-11	1.66
^{*152}Gd	8.258D-14	0.03
^{156}Dy	6.448D-13	0.65
^{158}Dy	4.439D-13	0.26
^{162}Er	1.231D-12	0.78
^{*164}Er	3.792D-12	0.20
^{168}Yb	3.792D-12	2.75
^{174}Hf	2.802D-12	1.96
^{*180}Ta	2.261D-15	0.18

Table 3—Continued

Isotope	GCE	(GCE/Solar)
^{180}W	4.416D-12	4.48
^{184}Os	7.157D-13	1.42
^{190}Pt	6.640D-13	0.64
^{196}Hg	8.884D-12	1.65

$^{(*)}$ – Isotopes pointed with * have to be excluded from the p-only list, as discussed by TRV11.

Table 4. Galactic chemical evolution of s-nuclides with important p-contribution

Isotope	GCE	(GCE/solar)
^{80}Kr	5.610D-10	0.20
^{86}Sr	1.692D-09	0.31
^{90}Zr	5.734D-09	0.43
^{96}Zr	8.258D-10	1.08

$^{(*)}$ – Isotopes pointed with * have to be excluded from the p-only list, as discussed by TRV11.